J. Fluid Mech. (1993), *vol.* 249, *pp.* 261–285

Manipulation of free shear flows using piezoelectric actuators

By JOHN M. WILTSE[1] AND ARI GLEZER[2]

[1] Department of Aerospace and Mechanical Engineering, The University of Arizona, Tucson, AZ 85721, USA

[2] Woodruff School of Mechanical Engineering, Georgia Institute of Technology, Atlanta, GA 30332, USA

(Received 6 December 1991 and in revised form 12 August 1992)

An air jet emanating from a square conduit having an equivalent diameter of 4.34 cm and a centreline velocity of 4 m/s is forced using four resonantly driven piezoelectric actuators placed along the sides of the square exit. Excitation is effected via amplitude modulation of the resonant carrier waveform. The flow is normally receptive to time-harmonic excitation at the modulating frequency but not at the resonant frequency of the actuators. When the excitation amplitude is high enough, the excitation waveform is demodulated by a nonlinear process that is connected with the formation and coalescence of nominally spanwise vortices in the forced segments of the jet shear layer. As a result, the modulating and carrier wave trains undergo spatial amplification and attenuation, respectively, downstream of the exit plane. Strong instabilities of the jet column are excited when the jet is forced at phase relationships between actuators that correspond (to lowest order) to the azimuthal modes $m = 0$, ± 1, ± 2, and -1 of an axisymmetric flow. The streamwise velocity component is measured phase locked to the modulating signal in planes normal to the mean flow. Resonantly driving the actuators with different carrier amplitudes results in a distorted mean flow having a featureless spectrum that can be tailored to provide favourable conditions for the introduction and propagation of desirable low-frequency disturbances.

1. Introduction

The introduction of low-level time-harmonic excitation at or near the boundaries of shear flows has been widely used as an important diagnostic tool for the study of individual instability modes in the broad disturbance spectrum of these flows (e.g. Ho & Huerre 1984). Moreover, the use of time-harmonic excitation provides a powerful tool for the manipulation of these instability modes, with dramatic effects on some of the global properties of the mean flow. For example, Oster & Wygnanski (1982) discovered that forcing a two-dimensional turbulent shear layer produces a 'frequency-locked' region in which growth is inhibited, the primary vortices are equally spaced, and their passage frequency is equal to the forcing frequency. Roberts & Roshko (1985) reported that when the frequency locking occurred downstream of the mixing transition, forcing could either enhance or reduce mixing and correspondingly alter the amount of reaction product. In addition to open-loop manipulation by periodic (normally harmonic) excitation, there have also been a number of investigations involving some degree of feedback control (e.g. Wehrmann 1967*b*; Liepmann & Nosenchuck 1982; Lee & Reynolds 1985; and Reisenthel 1988).

Suitable actuators having fast dynamic response and preferably low power consumption are the foundation of any scheme for the manipulation and control of flow instabilities. Most frequently, actuators have had mechanically moving parts, such as vibrating ribbons, movable flaps, or loudspeakers. Schubauer & Skramstad (1947) used a vibrating ribbon to excite Tollmien–Schlichting (T–S) waves across the span of a flat-plate boundary layer. Oster & Wygnanski (1982) excited two-dimensional instability modes in a plane mixing layer using a small oscillating spanwise flap mounted at the trailing edge of the flow partition. Crow & Champagne (1971) studied the axisymmetric mode $m = 0$ of a round jet using a plenum-mounted loudspeaker. A circular array of loudspeakers (Strange & Crighton 1983) and electromagnetic elements (Betzig 1981) placed around the perimeter of the jet nozzle have been used to excite azimuthal instability modes.

The shortcomings of the mechanical actuators described above have led to the development of two-dimensional mosaics of individually controlled surface-mounted heating elements. Surface heaters typically have a high frequency response with no moving parts, can be easily mounted on non-planar flow boundaries with relatively small intrusion to the flow, and can be used to output complex spatial/temporal excitation waveforms. The effect of time-dependent surface heating was used by Liepmann, Brown & Nosenchuck (1982) to introduce a controlled vorticity distribution into the adjacent boundary layer by exploiting the temperature dependence of the viscosity of the boundary-layer fluid. These experiments demonstrated the capability of surface-mounted heating elements to suppress harmonically excited T–S waves in a flat-plate boundary layer. The excitation of a free shear flow via an upstream boundary layer is bandwidth limited and, furthermore, may not be effective if the induced waves decay appreciably before reaching the downstream edge of the flow boundary. Despite this limitation, Nygaard & Glezer (1991) used a spanwise array of surface heaters to manipulate two- and three-dimensional vortical structures in a plane shear layer.

Piezoelectric actuators have many of the attributes of surface heaters but require significantly less power. These actuators have been successfully employed in a number of experiments. Wehrmann (1967*b*) implemented a feedback controller in a flat-plate boundary layer by using wall-mounted piezoelectric actuators to suppress naturally occurring T–S waves. Wehrmann (1965, 1967*a*) and Berger (1967) studied the wake of a piezoelectric cylinder having an oblong cross-section. Time-harmonic forcing was obtained by either slight deformation of the cylinder's cross-section (Wehrmann) or by spanwise-symmetric vertical bending of the cylinder along its axis (Berger). A feedback controller was used to synchronize vortex shedding to the excitation frequency. The authors also reported that vortex shedding could be suppressed at some Reynolds numbers.

The use of piezoelectric actuators for flow manipulation apparently has been limited because of the diminution in their response outside a narrow frequency band around their resonance frequency. The present manuscript describes a new technique which overcomes this difficulty and allows for effective manipulation of turbulent shear flows over a broad frequency range.

The utility of this technique has been demonstrated in a square air jet. A non-circular geometry was chosen because of its importance to technological applications in combustion (e.g. Gutmark *et al.* 1989). In experimental investigations of unforced non-circular jets in the absence of combustion, nozzle cross-sections were elliptical (Ho & Gutmark 1987; Hussain & Husain 1989), rectangular with various aspect ratios (Sforza, Steiger & Trentacoste 1966; Trentacoste & Sforza 1967), square

(DuPlessis, Wang & Kahawita 1974; Quinn & Militzer 1988), or triangular (Gutmark *et al.* 1985). Other investigations also considered the effect of various contraction shapes on the evolution of the ensuing jets (Tsuchiya, Horikoshi & Sato 1986). The studies mentioned above were primarily concerned with mean properties of the flow, such as spreading rates and time-averaged distributions of streamwise velocity and turbulent intensity.

The interest in non-circular jets for mixing and combustion applications stems from the fact that these jets typically entrain more ambient fluid than round jets having the same exit area and linear momentum flux (e.g. elliptic jets (Ho & Gutmark 1987) and square jets (Quinn & Militzer 1988)). Furthermore, the presence of sharp corners in the nozzles of reacting jets leads to the appearance of azimuthal concentrations of small-scale motions within the ensuing vortical structures, with considerable enhancement of mixing and reaction of the chemical species (Gutmark *et al.* 1989). Similar to plane mixing layers (Nygaard & Glezer 1991), these small-scale motions may be associated with the appearance of secondary streamwise vortices owing to azimuthal variations in the curvature of the primary (vortex ring-like) structures that are induced by the nozzle geometry.

The present manuscript describes the excitation of an air jet emanating from a square conduit using four individually controlled piezoelectric actuators placed along the sides of the square exit. A description of the air jet facility in which the research was conducted is given in §2. The excitation technique, the experimental results, and concluding remarks are presented in §§3, 4, and 5, respectively.

2. Experimental apparatus and procedure

2.1. *The air jet facility*

The air jet facility is shown in figure 1. The jet is driven by an axial blower (325 cfm) powered by a DC motor. Jet velocities up to 8 m/s can be realized. The blower is equipped with heating and cooling units (not shown), which allow for temperature control of the air jet. The blower is connected to a primary plenum equipped with a loudspeaker for excitation of axial instability modes in the jet column. The main part of the jet facility is constructed from several sections of Plexiglas tube, each 15.24 cm in diameter. The first two sections downstream of the plenum are fitted with screens, honeycomb, and foam material to eliminate swirl and reduce velocity fluctuations. The jet emanates from a 3.81 cm (1.5 in.) square aluminium conduit 57 cm long. The equivalent diameter (defined as the diameter of a round pipe having the same cross-sectional area) of the conduit is $D_e = 4.34$ cm. The conduit is centrally mounted on the downstream endplate of the Plexiglas tube and protrudes 35 cm in the upstream direction. The outer surfaces of the conduit are bevelled near its upstream end. No contraction is used, and an azimuthally uniform gap along the perimeter of the front endplate is adjusted until the velocity distribution across the Plexiglas tube upstream of the inlet of the square conduit is approximately uniform. This geometry helps to minimize secondary flow at the inlet and along the corners of the square conduit.

The streamwise velocity component is measured with a single hot-wire probe mounted on a computer-controlled three-axis traversing mechanism. When the jet is forced, the measurements are taken phase-locked to the excitation signal. The measurements reported in the present manuscript are taken on a 16×16 square grid in the (y, z)-plane at four streamwise positions, corresponding to $x/D_e = 1$, 2, 3, and 4. The spacing between adjacent grid points increases linearly with downstream

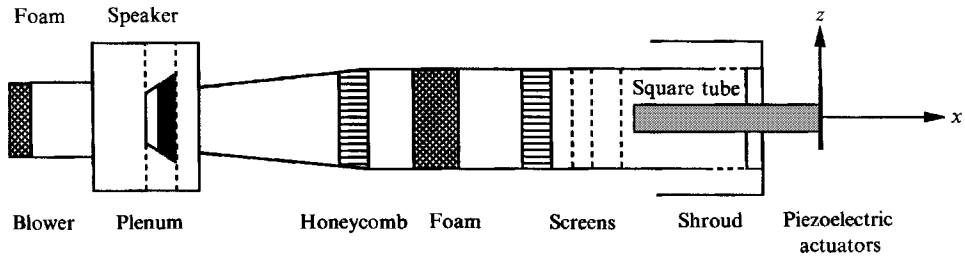

FIGURE 1. The air jet facility.

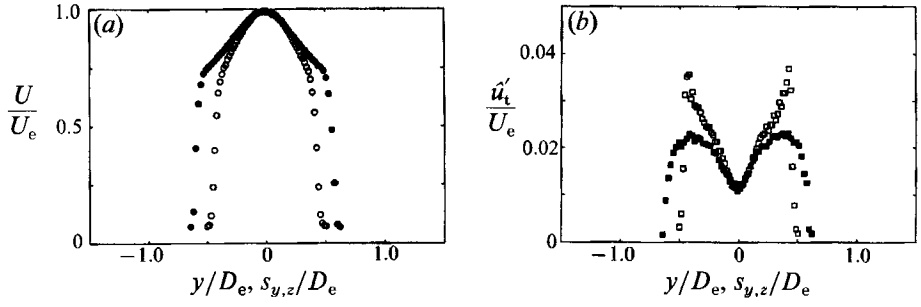

FIGURE 2. Profiles of (a) U/U_e and (b) $\hat{u}_t'/U_e$ measured at $x/D_e = 0.25$ along $z = 0$ (○ and □) and $z = y$ (● and ■).

distance to compensate for the spreading of the jet, and the width of the grid, $w_{y,z}(x)$, increases from 4.85 cm at $x/D_e = 1$ to 6.8 cm at $x/D_e = 4$. The lowest velocity of the unforced jet around the outer edges of the grid is approximately $0.1\,U_e$ (U_e is the jet centreline velocity at $x = 0$). A Masscomp laboratory computer system is dedicated to experiment control and data acquisition. A double-pass Schlieren system is used to visualize the flow when the jet fluid is heated 11 °C above the ambient temperature. The Schlieren view is in the (x,z)-plane and consists of a 15.2 cm diameter circle centred at $x/D_e = 1.75$ and $z = 0$.

2.2. *Experimental conditions*

In the present experiments, the time-averaged jet centreline velocity at $x = 0$ is $U_e = 4$ m/s, the Reynolds number based on D_e and U_e is 11000, and $\hat{u}_t'/U_e = 0.012$ at the centre of the jet exit, where $\hat{u}_t'(\boldsymbol{x})$ is the time-averaged r.m.s. velocity fluctuations. We note that in the present manuscript time series of turbulent fluctuations of the streamwise velocity component $u_t'(\boldsymbol{x}, t)$ are calculated from instantaneous velocity records (Glezer, Katz & Wygnanski 1989). This technique uses a digital high-pass filter and is extremely effective in discriminating between small-scale streamwise motions and spurious contributions from low-frequency variations of the flow relative to its mean. Profiles of $U(\boldsymbol{x})$ and $\hat{u}_t$ measured at $x = 1.08$ cm ($x/D_e = 0.250$) are shown in figures 2(*a*) and 2(*b*), respectively. These profiles are measured along $z = 0$ and along $z = y$ (hereinafter referred to as the wall bisector and the corner bisector of the square conduit, respectively). The symmetry of these profiles with respect to the jet centreline (x-axis) is indicative of the symmetry of corresponding profiles of the flow within the square conduit.

The length of the square duct is chosen so that the distribution of the time-averaged streamwise velocity at the exit plane is almost fully developed and the

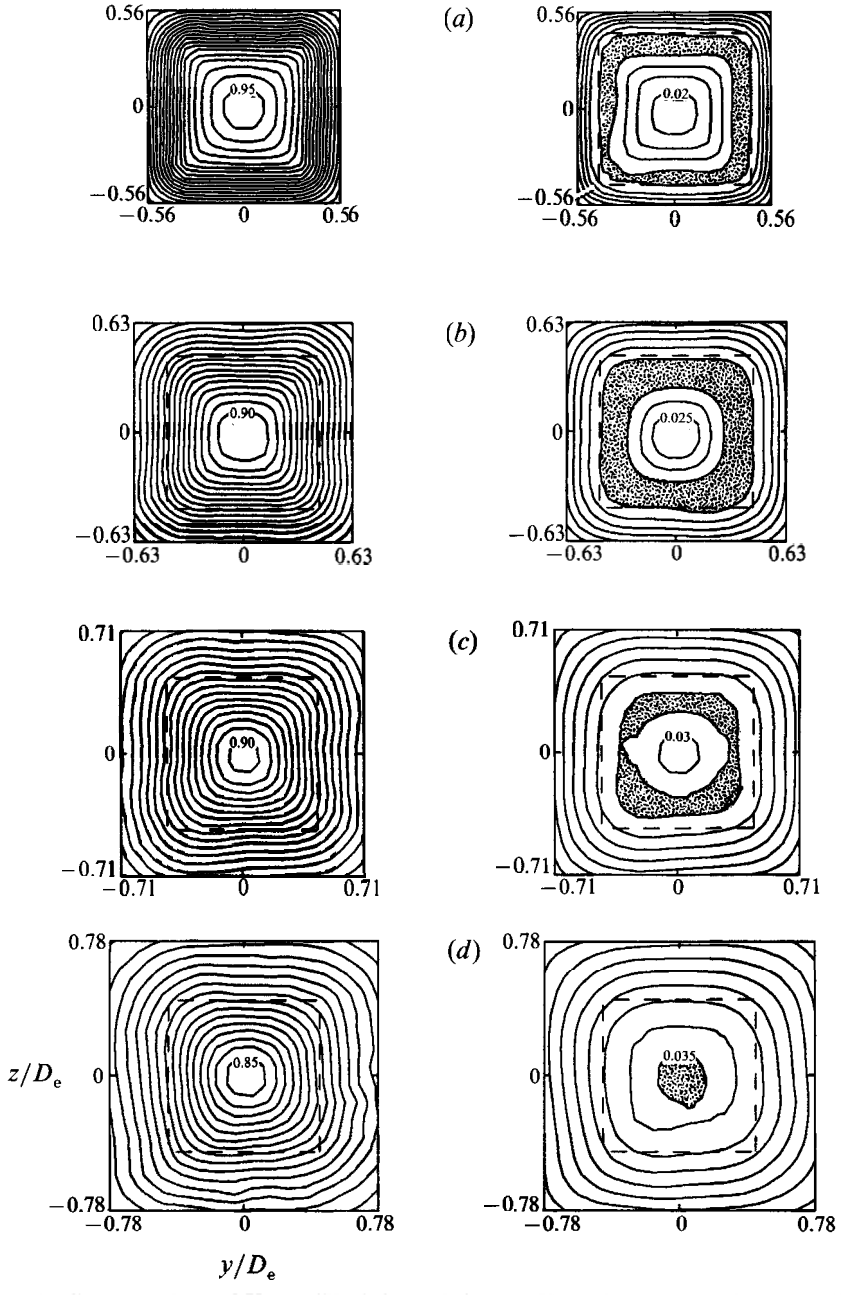

FIGURE 3. Contour plots of $U(y,z)/U_e$ (left) and $\hat{u}'_t(y,z)/U_e$ (right) measured at (*a*) $x/D_e = 1$, (*b*) 2, (*c*) 3, and (*d*) 4. Contour increments for U/U_e and $\hat{u}'_t/U_e$ are 0.05 and 0.005, respectively; levels of centre contours are labelled. Regions where $\hat{u}'_t/U_e$ is greater than the maximum contour level are shaded. The dashed lines denote the extent of the jet exit.

secondary flow at the corners is minimal. The time-averaged centreline velocity within a square duct typically increases with downstream distance from the duct inlet due to the increase in the thickness of the wall boundary layers. The centreline velocity reaches a maximum at some distance from the inlet before it begins to decrease owing to the evolution of secondary flow in the corners (Melling & Whitelaw

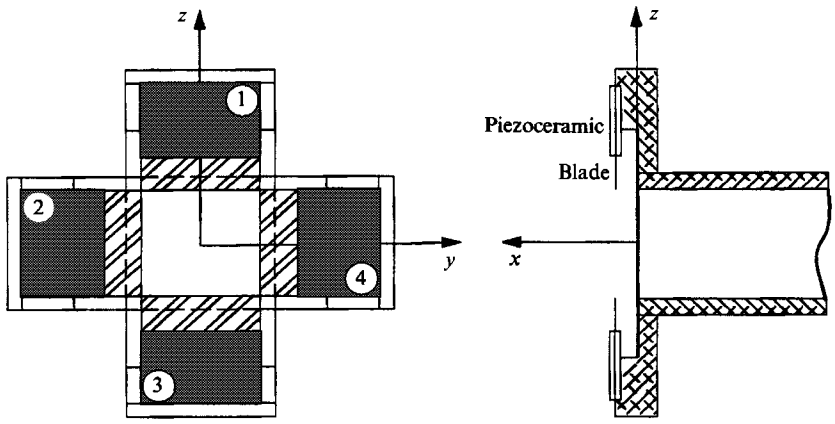

FIGURE 4. Schematic diagram showing placement of actuators.

1976). The measurements of Gessner, Po & Emery (1977), in a square duct at $Re_{D_e} = 2.21 \times 10^5$, show that the mean centreline velocity has a maximum at $x/D_e \approx 35$ (measured from the inlet of the duct) and diminishes to a lower level at $x/D_e \approx 53$ (ostensibly where the corner flow becomes fully developed). Although the experiments of Gessner *et al.* were conducted at a higher Reynolds number than the present experiments, there is a remarkable similarity between their mean velocity profiles at $x/D_e \approx 35$ and the profiles of figure 2 (*a*, *b*). That the secondary flow in the corners is less developed than the flow in the wall boundary layers is indicated by the lower levels of $\hat{u}_t'$ near the corners with respect to those near the wall midpoints (figure 2*b*). The measurements of Melling & Whitelaw show that the appearance of secondary corner flow is accompanied by sharp peaks of $\hat{u}_t'$ near the corners.

Figure 3 (*a–d*) shows pairs of contour plots of U/U_e and $\hat{u}_t'/U_e$ (contour increments are 0.05 and 0.005, respectively) in the (y, z)-planes at $x/D_e = 1$, 2, 3, and 4. The dashed lines denote the transverse extent of the jet exit (3.81 cm square). These contour plots demonstrate that the jet largely retains its initial squareness within the streamwise domain of the present measurements. Furthermore, the distributions of r.m.s. velocity fluctuations suggest that, at least for the unforced square jet, the nozzle corners (or secondary corner flow within the square duct) do not contribute to localized azimuthal enhancement of small-scale motion. Similar results were also reported by Gutmark *et al.* (1985) for a jet emanating from a square duct at a much higher Reynolds number ($Re \approx 63000$).

2.3. *Piezoelectric actuators*

The jet is forced using four piezoelectric actuators (such actuators are commercially available) that are placed along the sides of the square exit (figure 4). Each actuator is a composite of a thin (0.013 cm) stainless steel blade 3.81 cm wide and 3 cm long that is partially sandwiched along its width between two rectangular overlapping plates of piezoelectric ceramic (each measuring $3.8 \times 1.9 \times 0.018$ cm). Conducting electrodes are deposited on the major faces of each piezoelectric plate, and the plates are polarized in opposite directions. The composite end of each actuator is rigidly fixed along its width so that approximately 80% of its length is cantilevered. When an electric field is applied across the two outer electrodes of the actuator, the actuator bends about its fixed end. The magnitude and direction of the displacement of the free end is nominally uniform and depends on the magnitude and polarity of

the applied voltage. The direction of tip displacement reverses with the polarity of the applied voltage. The largest tip displacement is achieved when the actuator is driven with a time-harmonic voltage at a resonant frequency, ν_r, which depends primarily on the resonance characteristics of the piezoelectric plates and their cantilevered length, the thickness and length of the stainless steel blade, and the rigidity of the actuator mounting.

In the present experiments, the actuators are placed along the sides of the square exit in the plane $x/D_e = 0.11$ so that the tip of each blade is aligned with the respective inner surface of the square conduit. The actuators have virtually no effect on the flow when they are not in use. The resonant frequencies of the actuators are not identical and vary within 500 ± 20 Hz. The motion of the actuators is parallel to the jet axis, and their maximum peak-to-peak displacement at 22 V r.m.s. is approximately 1 mm (measured using stroboscopic illumination). Below this maximum, the actuators' peak-to-peak displacements vary almost linearly with the amplitude of the input voltage. We note that for a given input amplitude there is a substantial diminution in the actuators' displacements outside a narrow band around their resonance frequencies.

3. Amplitude-modulated excitation

The limited utility of piezoelectric actuators outside a narrow frequency band around their resonance frequency can be overcome by implementing a new excitation technique in which the actuators are resonantly driven with a time-harmonic carrier wave train that is *amplitude modulated* with the desired excitation waveform. The resonant frequency of the piezoelectric actuators is selected to be well above the frequency band to which the flow is normally receptive. The premise is that, provided velocity perturbations induced by the actuators are large enough, the excitation waveform is effectively demodulated by exploiting flow nonlinearities. Because the flow is not receptive to excitation at the carrier frequency and its higher harmonics, these disturbances are attenuated downstream of the actuators while the modulating wave train is effectively amplified by the flow.

In the present experiments excitation is effected by the motion of the free ends of cantilevered actuators (§2) that induce streamwise velocity perturbations, $u_p(\boldsymbol{x}, t)$, in (nominally plane) segments of the jet shear layer. Each actuator is resonantly driven with a carrier waveform, $e_i(t)$ $(i = 1, 2, 3, 4)$, which is amplitude modulated with a time-harmonic wave train, $e_m^i(t)$:

$$e_i(t) = e_m^i(t)\, A_r^i \sin(\omega_r^i t),$$

where

$$e_m^i(t) = [1 + \epsilon_i \sin(\omega_f^i t + \Phi_i)],$$

A_r^i is the amplitude of the carrier signal, ϵ_i is the degree of modulation $(0 \leqslant \epsilon_i \leqslant 1)$, $\nu_f^i = \omega_f^i/2\pi$ is the modulating frequency (which is also the desired excitation frequency), $\nu_r^i = \omega_r^i/2\pi$ is the carrier frequency (or the resonance frequency of the actuator), and Φ_i is the phase of $e_m^i(t)$ relative to a time-harmonic reference wave train at the modulating frequency. Each actuator is driven by a dedicated AM signal generator, and the modulating waveforms are generated by the laboratory computer via a D/A interface. We note that the actuators can also be driven with anharmonic modulating waveforms.

The excitation amplitude and degree of modulation of each actuator are measured on the jet centreline (at $x/D_e = 0.11$) without flow using a broadband miniature

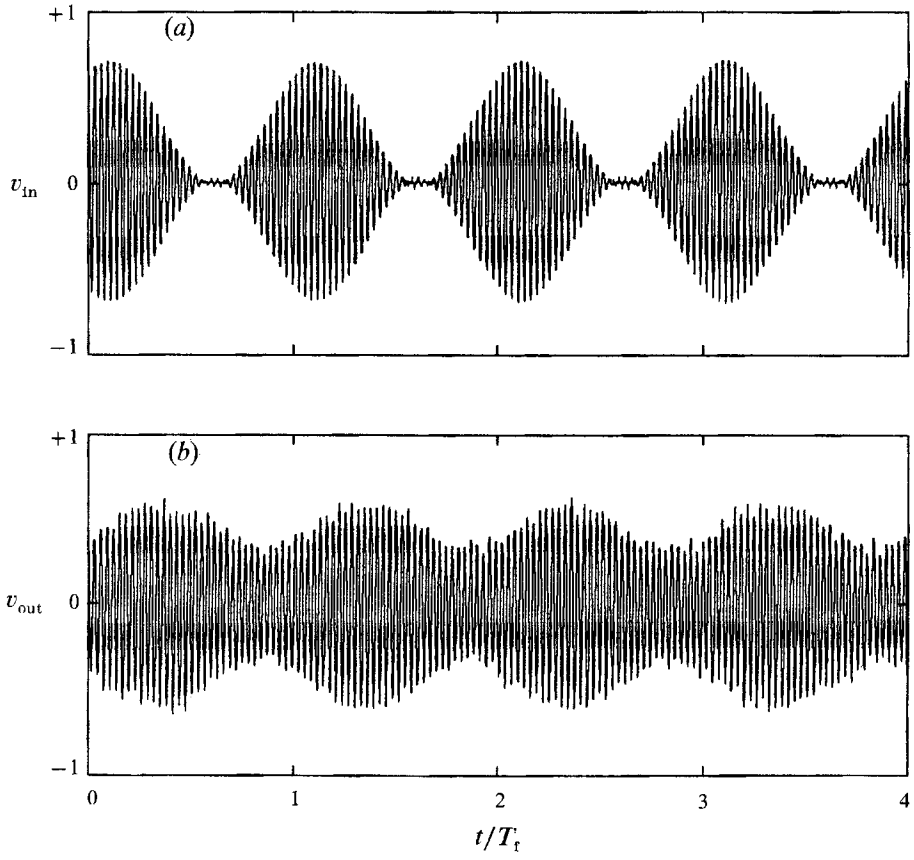

FIGURE 5. (*a*) Excitation waveform input and (*b*) corresponding pressure fluctuations measured by a microphone ($\nu_r = 500$ Hz, $\nu_f = 16$ Hz).

microphone. Figure 5 shows the input excitation waveform and the corresponding pressure fluctuations measured by the microphone ($\nu_r = 500$ Hz, $\nu_f = 16$ Hz). Although the degree of modulation of the input signal is $\epsilon = 1$, the degree of modulation of the measured waveform $\tilde{\epsilon}$ is approximately 0.33. The diminution in the degree of modulation of the measured waveform is clearly related to a characteristic response time that is associated with the equivalent capacitance, inductance, and resistance of the piezoelectric material and the mechanical inertia of the actuator in resonance conditions. In the present experiments, the characteristic rise time in response to a unity step in the degree of modulation (i.e. $\epsilon = H(t)$, where $H(t)$ is a Heaviside function) is approximately 35 ms.

Since at resonance the streamwise displacement of the free end of the actuators (relative to the rest position) is proportional to $e_i(t)$, it follows that for $\omega_f^i \ll \omega_r^i$, the amplitude of the perturbation velocity at the free end of each actuator, u_p^i, is proportional to $A_r^i \omega_r^i$. Thus, substantial velocity perturbations can be achieved even if A_r^i is small but ω_r^i is large. (The maximum amplitude of the perturbation velocity in the present experiments is estimated to be 3 m/s.) While the spectral components of u_p^i are limited to ν_r^i and its two sidebands $\nu_r^i \pm \nu_f^i$, a quadratic nonlinearity in the flow can lead to spectral components at ν_f^i, $2\nu_f^i$, $2\nu_r^i$, $2\nu_r^i \pm \nu_f^i$, and $2\nu_r^i \pm 2\nu_f^i$. Because the flow is not receptive to excitation at ν_r and its higher harmonics, these frequencies should be rapidly attenuated with downstream distance.

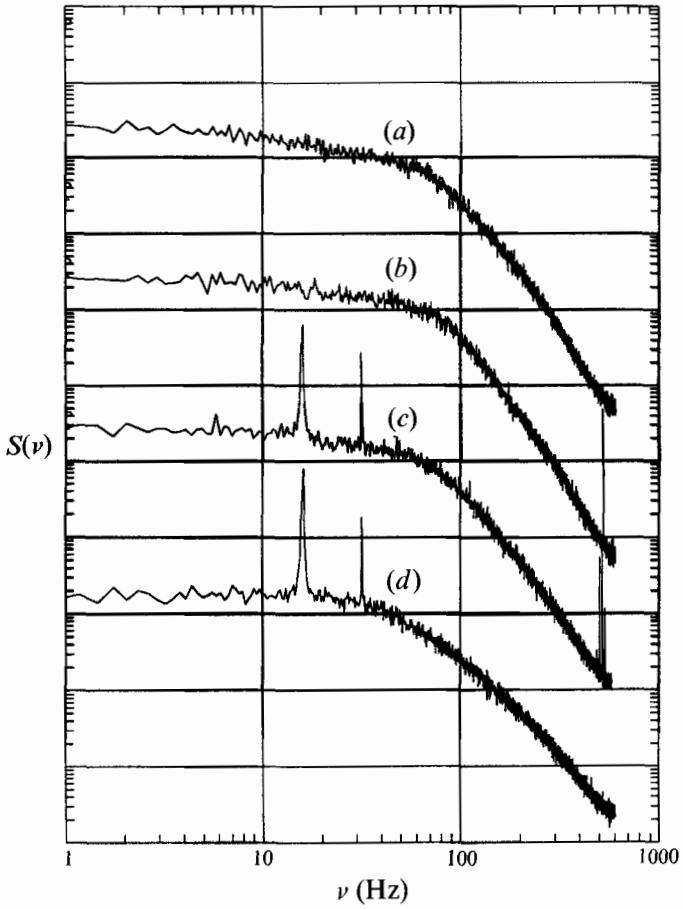

FIGURE 6. Power spectra $S(\nu)$ of the streamwise velocity at $y = 0$, $z = 1.91$ cm, and $x/D_e = 0.23$: (*a*) unforced; (*b*) forced using actuator 1 with unmodulated carrier [$\nu_r^1 = 510$ Hz]; (*c*) as for (*b*) but with amplitude modulation ($\nu_f^1 = 16$ Hz, $\tilde{\epsilon} = 0.33$); (*d*) as for (*c*) but at $x/D_e = 1$.

Figure 6 shows power spectra, $S(\nu)$, obtained from hot-wire measurement of streamwise velocity in the jet shear layer at $y = 0$, $z = 1.91$ cm (the elevation of the free end of actuator 1), at two streamwise stations $x/D_e = 0.23$ (curves *a*–*c*) and $x/D_e = 1$ (curve *d*). A power spectrum of the unforced jet is shown as curve (*a*) for reference, and for curves (*b*–*d*) the flow is forced with actuator 1. When $\epsilon_1 = 0$, the jet shear layer is forced at the carrier (resonance) frequency $\nu_r^1 = 510$ Hz (curve *b*), which is prominent in this otherwise featureless spectrum. While the power spectra for curves (*a*) and (*b*) are similar at low frequencies, there is a small increase in spectral content above 70 Hz for curve (*b*), which indicates an increase in small-scale motions. The most striking feature in curve (*c*) ($\nu_f = 16$ Hz, $\tilde{\epsilon}_1 = 0.33$) is the presence of spectral components at the modulating frequency and its first harmonic, in addition to spectral components at the carrier frequency and its two sidebands (510 Hz, and 510 ± 16 Hz, respectively). This power spectrum shows that the excitation waveform is, in fact, demodulated by the flow. (Power spectra of the excitation input measured by a microphone on the centreline of the square conduit at $x/D_e = 0.11$ with no flow show only peaks at the carrier frequency and its two sidebands and contain no measurable power at the modulating frequency and its

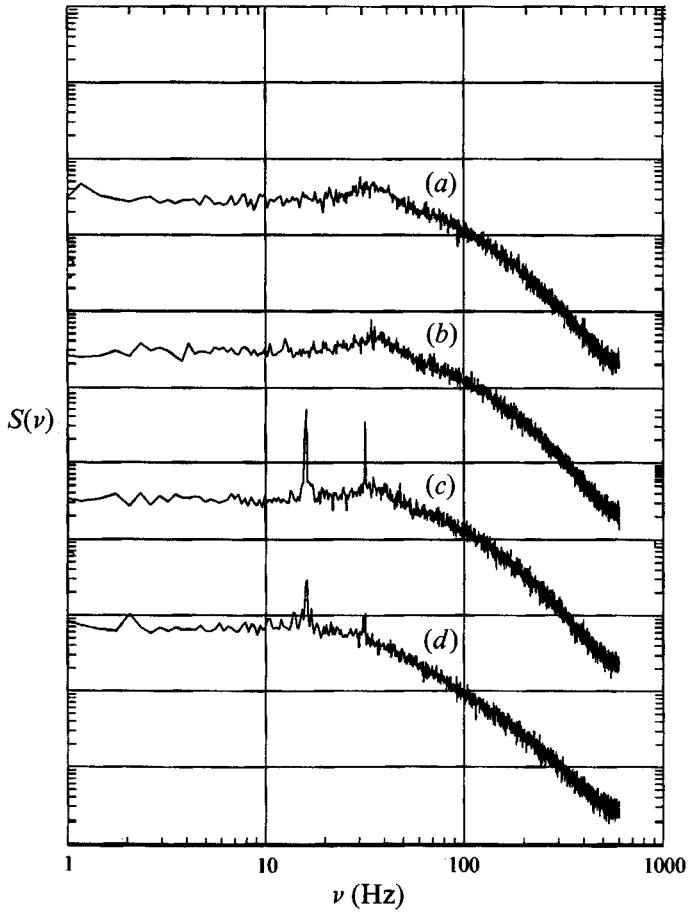

FIGURE 7. Power spectra $S(\nu)$ of the streamwise velocity at $y = z = 0$, $x/D_e = 1$: (*a*) unforced; (*b*) forced using all actuators with unmodulated carriers $[A_r^1 = A_r^2 = A_r^3 = A_r^4]$; (*c*) as for (*b*) but with amplitude-modulated carriers ($\tilde{\epsilon}_i = 0.33$, $\nu_f^i = 16$ Hz); (*d*) as for (*c*) but at $x/D_e = 4$.

higher harmonics.) At $x/D_e = 1$ (figure 6, curve *d*), the spectral components at the carrier frequency and its sidebands are absent, and the amplitude of the spectral component at 16 Hz is somewhat higher, which may be indicative of spatial amplification.

Figure 7 shows power spectra of the streamwise velocity component measured on the jet centreline at $x/D_e = 1$. The power spectrum of the unforced jet (curve *a*) has a broad peak around $\nu = 35$ Hz (corresponding to a Strouhal number $St_{D_e} = 0.38$). This spectrum is virtually unchanged when all four actuators are driven at their respective resonant frequencies with unmodulated carriers having the same excitation amplitudes (curve *b*). The excitation amplitude for most of the present experiments was chosen so that, when $\epsilon_i = 0$, the carrier frequency has virtually no effect on the mean structure of the jet. (In §4, we also discuss the capability of the actuators to substantially distort the mean flow when $\epsilon_i = 0$.) In figure 7, curve (*c*), the resonant waveform of each actuator is amplitude modulated with the same degree of modulation ($\tilde{\epsilon}_i = 0.33$) and modulating frequency ($\nu_f^i = 16$ Hz, $St_{D_e} = 0.174$). As in figure 6, curve (*d*), there are spectral peaks only at the excitation frequency and its first harmonic. These peaks are still apparent in power spectra measured at $x/D_e = 4$ (figure 7, curve *d*).

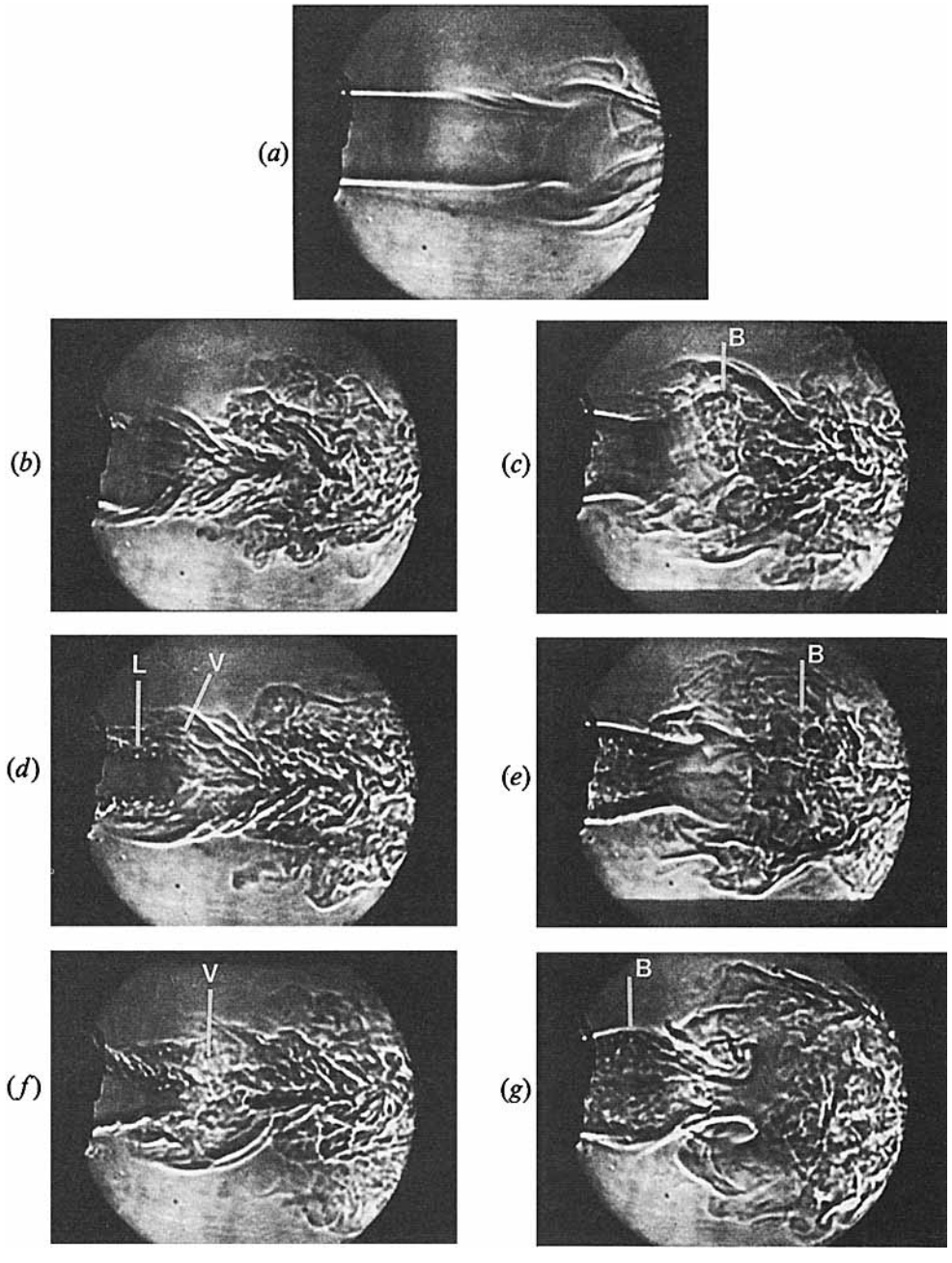

FIGURE 8. Schlieren photographs in the (x, z)-plane of the square jet ($0 \leqslant x/D_e \leqslant 3.5$): (*a*) unforced and (*b–g*) forced with amplitude-modulated carriers at $\nu_f = 12$ Hz. The jet is forced separately with actuators 1, 3 (*b*, *d*, *f*) and actuators 2, 4 (*c*, *e*, *g*) and photographed at three time intervals during the excitation period: $\tau = 0.03$ (*b*, *c*), 0.25 (*d*, *e*), and 0.47 (*f*, *g*).

Schlieren photographs of the forced jet in the (x, z)-plane are shown in figure 8(*a–g*). Each Schlieren view includes the exit plane of the jet (the flow is from left to right) and extends through $x/D_e = 3.5$. In order to demonstrate the effect of the actuators, the jet exit velocity is reduced to 2.75 m/s ($Re_{D_e} = 7700$). The unforced jet is shown for reference in figure 8(*a*), and it is noted that the jet shear layer becomes

unstable at $x/D_e > 1.75$. The jet is separately forced using pairs of opposite actuators (1, 3 in figure 8*b*, *d*, *f*; 2, 4 in figure 8*c*, *e*, *g*) and having identical time-harmonic modulating waveforms ($\nu_f = 12$ Hz). During the excitation period, T_f, the flow is illuminated by a strobe, which is triggered at a phase delay relative to the zero crossings of the modulating waveform. The effect of excitation with pairs of opposite actuators is photographed at the same phase delay (figures 8*b*, *c*, 8*d*, *e*, and 8*f*, *g*). Thus, each pair of photographs can be thought of as phase-locked views in the (x, z)- and (y, z)-planes. Figures 8(*b*, *c*), 8(*d*, *e*), and 8(*f*, *g*) are taken at $\tau = 0.03$, 0.25, and 0.47, respectively ($\tau = t/T_f$, and $\tau = 0.25$ roughly corresponds to the peak amplitude of the modulated carrier waveform).

A striking feature of figure 8(*d*) is the formation of rows of locally two-dimensional line vortices (marked L) with their axes parallel to the tips of actuators 1 and 3 (i.e. in the plane of figure 8*e*). These vortices are formed at the carrier (resonance) frequency ν_r^i, and their nominal cross-sectional dimension is of the order of the actuator displacement. Farther downstream from the nozzle, these vortices appear to roll into larger vortices (marked V in figure 8*d*, *f*) at the modulating frequency ν_f. The formation of these vortical structures, which apparently results from temporal modification of azimuthal vorticity in the jet shear layer by the actuators, suggests itself as the nonlinear mechanism necessary for the demodulation of the excitation wave train. For a given jet exit velocity, the rollup of vortices at the carrier frequency stops when the amplitude of the (modulated) excitation signal is below a given threshold (e.g. figure 8*b*). Hence, it appears that if the velocity perturbations induced by the tips of the actuators are high enough, the high-frequency rollup within the jet shear layer may be the result of a localized (inviscid) inflexional instability.

Another important consequence of the excitation is the substantial broadening of the jet in the x, y view (figure 8*c*, *e*, *g*). This broadening is apparently the result of a marked increase in the cross-stream spreading rates of the forced segments of the jet shear layer as seen in the (x, z)-plane (figure 8*d*, *f*). (It should be emphasized that since only the jet fluid is heated, much of the outer flow is not visualized.) Significant changes in the cross-stream spreading rate of forced plane mixing layers has been observed by a number of investigators. In particular, Champagne, Pao & Wygnanski (1976) reported that the cross-stream spreading of a one-stream plane mixing layer increases when its upstream boundary layer is tripped with a spanwise wire. In a related experiment, Oster, Wygnanski & Fiedler (1977) noted that their trip wire did not produce a fully developed turbulent boundary layer but did, in fact, induce measurable quasi-sinusoidal oscillations in the ensuing one-stream shear layer. Presumably the perturbations effected by the trip wire induced a premature rollup of the vortex sheet downstream of the flow partition, similar to the effect of the actuators in the present experiments. The coalescence of the high-frequency vortices into larger vortical structures when the excitation waveform is amplitude-modulated may be similar to the formation of spanwise vortices in a plane shear layer that is excited at a much lower frequency that its 'natural' rollup frequency (e.g. the 'collective interactions' discovered by Ho & Huang 1982 in a two-stream shear layer forced at a subharmonic of the natural frequency).

Figure 8(*f*) shows the substantial narrowing of the jet's core downstream of the exit plane when the excitation amplitude begins to drop below the level necessary for the formation of the line vortices. As a result of the appearance of these vortices, the jet 'bulges' in the (x, y)-plane (marked B in figure 8*g*). The 'bulge' continues to spread as it is advected in the streamwise direction and, when $\tau = 0.03$ in the next

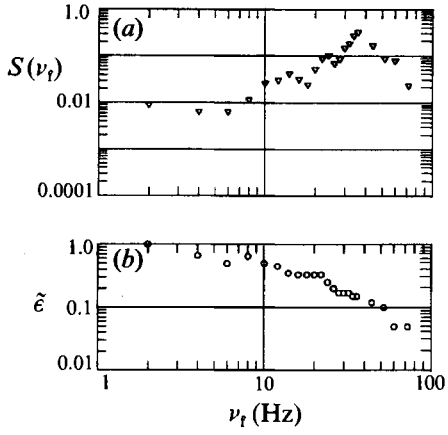

FIGURE 9. The response of the flow to amplitude-modulated excitation over a range of modulating frequencies: (*a*) $S(\nu_f)$; (*b*) $\tilde{\epsilon}(\nu_f)$.

excitation cycle, it is located at $x/D_e \approx 1.65$ (marked B in figure 8*c*). Note the location and width of the bulge in figure 8(*e*) during the rollup of the line vortices near the jet exit plane when $\tau = 0.25$ (figure 8*d*).

The combined response of the flow and the actuators to amplitude-modulated excitation over a range of modulating frequencies is deduced from power spectra, $S(\nu)$, of the streamwise velocity measured on the jet centreline at $x/D_e = 1$. Several runs over a range of modulating frequencies were made at fixed, identical input amplitudes, A_f^i. The degree of modulation of the excitation waveforms was measured on the jet centreline at $x/D_e = 0.11$ for each of the modulating frequencies. Figure 9 shows $S(\nu_f)$ for a range of forcing frequencies for which $S(\nu_f)$ is clearly above the background spectrum, and a corresponding plot of the measured degree of modulation, $\tilde{\epsilon}(\nu_f)$. Although $S(\nu_f)$ has a maximum at $\nu_f = 36$ Hz ($St_{D_e} = 0.39$), the flow effectively demodulates the excitation waveform between 2 and 75 Hz. The demodulation appears to be relatively insensitive to $\tilde{\epsilon}$, which is primarily affected by the time constant of the actuators (§2.3). We note that the nominal power required to drive each of the present actuators is less than 10 mW, and higher excitation amplitudes can be easily realized, if necessary, by increasing the amplitude of the input resonant waveforms to the actuators. There is no question that by proper adjustment of the excitation amplitudes, the jet can be effectively excited over a broad range of frequencies corresponding to an order-of-magnitude variation in the Strouhal number.

Finally, it should be mentioned that excitation can also be effected by frequency modulation of ω_r. As a result, the excitation amplitude is modulated according to the variation in the response of the actuator within its resonance bandwidth. The degree of modulation is determined by the amplitude and period of the modulating waveform.

4. Modification of the square jet

As discussed in §§2.3 and 3, excitation of the square jet is accomplished by amplitude modulation of the signals resonantly driving each of four piezoelectric actuators placed around the jet exit. In what follows the modulating waveforms are time-harmonic and have the same frequency, $\nu_f = 16$ Hz. The phase Φ_i of each of the modulating waveforms is varied relative to a time-harmonic reference signal, $e_{ref}(t)$

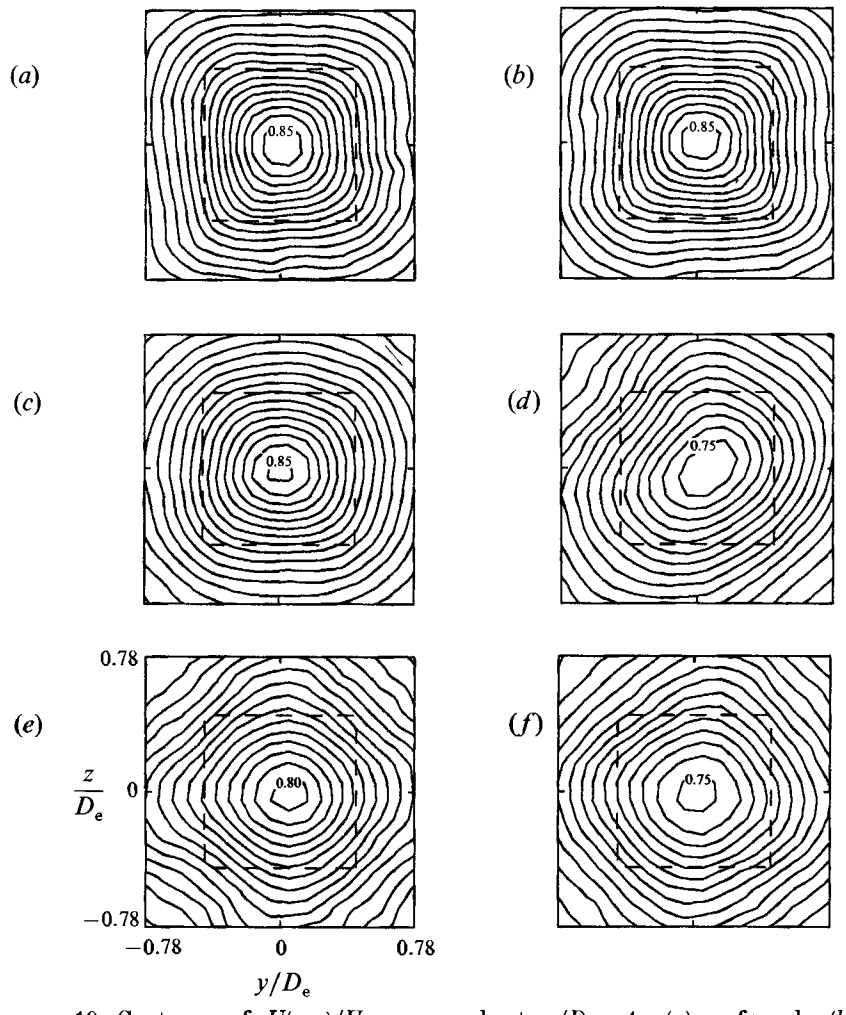

FIGURE 10. Contours of $U(y,z)/U_e$ measured at $x/D_e = 4$: (*a*) unforced; (*b*) forced with unmodulated carriers; (*c*) forced with P_0; (*d*) forced with $P_{\pm 1}$; (*e*) forced with $P_{\pm 2}$. Contour increments are 0.05, and the maximum contour levels are labelled.

(having the same frequency), to produce four excitation programmes: (*a*) $\Phi_i = 0$ $(i = 1,2,3,4)$; (*b*) $\Phi_1 = \Phi_2 = 0$, $\Phi_3 = \Phi_4 = \pi$, (*c*) $\Phi_1 = \Phi_3 = 0$, $\Phi_2 = \Phi_4 = \pi$, and (*d*) $\Phi_i = (i-1)\pi/2$ $(i = 1,2,3,4)$. We note that the phase relationships between the modulating waveforms for programmes *a*, *b*, *c*, and *d* correspond (to lowest order) to azimuthal modes $m = 0, \pm 1$, and ± 2 and spinning mode $m = -1$ of an axisymmetric jet. These programmes will be hereinafter referred to as P_0, $P_{\pm 1}$, $P_{\pm 2}$, and P_{-1}, respectively.

4.1. *Distortion of the mean flow*

The azimuthal distortion of the forced flow as a result of the excitation programmes outlined above is shown in y, z contour plots of normalized mean streamwise velocity at $x/D_e = 4$ (figure 10*a–f*). Figure 10(*a*) (unforced jet, the same as figure 3*d*) is included for reference. In figure 10(*b*), the jet is forced with unmodulated carrier signals (i.e. $\epsilon_i = 0$) each at the resonance frequency of the respective actuator. As noted in §3, although the carrier frequencies are present in velocity spectra measured near the actuators (cf. figure 6, curve *b*), the excitation amplitudes of the

unmodulated input signals are chosen so that the mean flow is not distorted within the domain of measurements considered here. This excitation level is below the level necessary for rollup of the azimuthal line vortices within the jet shear layer. We note for reference below that excitation with unmodulated carrier signals of higher amplitudes can result in a distorted mean flow having essentially a featureless spectrum.

Excitation with P_0 (figure 10*c*) results in a mean flow that resembles a round jet (unforced square jets normally become round much farther downstream). In figure 10(*d*), the jet is forced with $P_{\pm 1}$. The jet's cross-section becomes almost oval and is stretched along the corner bisector, which is the line of symmetry of the forcing. When the square jet is forced with $P_{\pm 2}$, its cross-section has an approximate fourfold symmetry, where the y- and z-axes are the axes of symmetry (figure 10*e*). The jet's cross-section is almost equally stretched along each of these axes. Although it appears that when the jet is forced with $P_{\pm 2}$ the distortion of the mean flow is approximately equivalent to a 90° rotation of the original square jet, measurements at $x/D_e = 1$, 2, and 3 do not show evidence of such rotation. In fact, the radial stretching of the mean cross-section of the forced jet is the result of azimuthally non-uniform spreading of the jet shear layer. Finally, the result of forcing with P_{-1} is similar to a combination of forcing with P_0 and $P_{\pm 2}$ (figure 10*e*). The jet appears to be rounded, as with P_0, yet there is some stretching, as with $P_{\pm 2}$.

We note in passing that interaction between two oppositely spinning modes having the same wavenumber and frequency in a round jet can lead to a triad resonance that distorts the mean flow with azimuthal periodicity of twice the mode number. For example, excitation of modes ± 1 results in $\cos(2\phi)$ distortion (where ϕ is the azimuthal coordinate) of the normally circular mean velocity contours and, similarly, excitation of modes ± 2 results in a $\cos(4\phi)$ distortion of the mean velocity contours (Long & Petersen 1992). Modal decomposition of the ensemble-averaged time series of the streamwise velocity $\langle u(\boldsymbol{x}, t)\rangle$ (not shown) demonstrates that each of the excitation programmes $P_{\pm 1}$ and $P_{\pm 2}$ leads to the appearance of oppositely spinning azimuthal modes $m = \pm 1$ and ± 2, respectively, in addition to a weak mode $m = 0$. The presence of these modes explains the azimuthally periodic distortion of the mean flow in figures 10(*d*) and 10(*e*). We also note that excitation with P_0 results in the appearance of a strong mode $m = 0$, as manifested in the circular distortion of the mean flow in the (y, z)-plane $x/D_e = 4$ (figure 10*c*). Finally, excitation with P_{-1} results in a spinning mode $m = -1$ with weaker spurious modes $m = 1$ and 3.

The distortion of the jet due to excitation with carrier waveforms having azimuthally non-uniform amplitudes is shown in figures 11(*a*) and 11(*b*). Similar to figure 10(*a–f*), figures 11(*a*) and 11(*b*) are y, z contour plots of the mean streamwise velocity at $x/D_e = 4$. In figure 11(*a*), the excitation waveforms are unmodulated, with the amplitudes of actuators 1 and 3 being twice the amplitudes of actuators 2 and 4 (i.e. $A_r^1 = A_r^3 = 2A_r^2 = 2A_r^4$). At this excitation level, the jet is highly distorted, with an apparent aspect ratio slightly in excess of two. We note that the excitation amplitudes of actuators 1 and 3 are above the threshold at which line vortices roll up at the carrier frequency within the forced azimuthal segments of the jet shear layer (cf. figure 8*d*). Because the excitation leads to an increase in the cross-stream spreading of the jet shear layer, the jet cross-section distorts and becomes rectangular compared to the cross-section of the unforced jet in figure 10(*a*). The centreline velocity of the forced jet is $0.75U_e$ compared to $0.85U_e$ in the unforced jet.

Schlieren visualization suggests that in the absence of low-frequency modulation of the excitation waveforms, the line vortices in the forced azimuthal segments of the

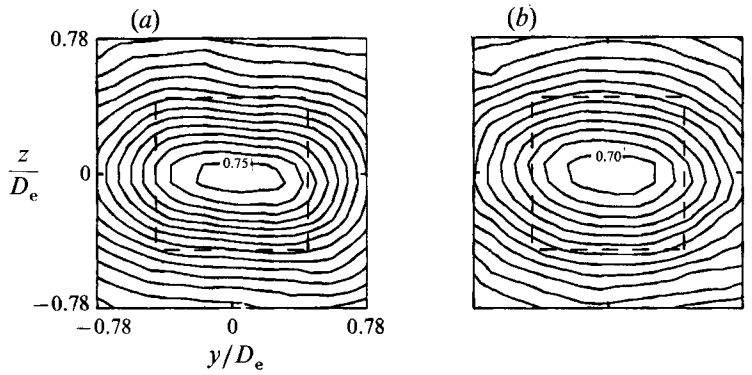

FIGURE 11. As in figure 10 except that $A_r^1 = A_r^3 = 2A_r^2 = 2A_r^4$: (*a*) unmodulated; (*b*) amplitude-modulated with P_0.

jet shear layer rapidly coalesce and lose their identity. In fact, spectra of the streamwise velocity measured on the jet centreline at $x/D_e = 1$ (not shown) are essentially featureless and very similar to the spectrum shown in figure 7, curve (*a*). Hence, by driving the actuators with carrier signals of different amplitudes, the azimuthally non-uniform spreading of the jet shear layer can be exploited to provide a distorted mean base flow to which various low-frequency disturbances can be added by appropriate amplitude modulation and phase selection of the modulating waveforms. In figure 11(*b*), the carrier waveforms of the actuators are amplitude-modulated with P_0 and the cross-section of the jet becomes oval. This capability further suggests that proper selection of input waveforms can be used to tailor the mean velocity profile so as to provide favourable conditions for the introduction and propagation of desirable low-frequency disturbances.

4.2. *Phase-averaged flow structure*

The most prominent feature of non-circular jets is that the variation of their radial spreading in the streamwise direction is azimuthally non-uniform. In fact, the radial spreading of the jet is larger in azimuthal positions where the curvature of the jet boundary has a local minimum. (The jet boundary may be defined by contours of time-averaged streamwise velocity in (y,z)-planes along the jet axis.) These azimuthal variations in jet spreading can be accompanied by significant variations in radial entrainment of ambient fluid, as was demonstrated by Ho & Gutmark (1987) in an elliptic jet having an aspect ratio of 2:1. Because the streamwise spreading rate of a non-circular jet is larger where the azimuthal curvature of its boundary is smaller, the (y,z)-cross-section of the jet distorts with downstream distance. In the case of an elliptic jet, the major and minor axes of the jet's cross-section are interchanged several times with downstream distance (Ho & Gutmark) because the streamwise spreading rate of the jet is larger in the plane of the minor axis.

Previous investigations of non-circular jets have mostly emphasized time-averaged measurements, and the dynamical evolution of the flow in question has been inferred from flow visualization. In this section we discuss the phase-averaged flow structure with particular attention to the excitation programme $P_{\pm 2}$.

In figures 12(*a–d*) for P_0 and 13(*a–d*) for $P_{\pm 2}$, we show four pairs of y,z contour plots of the phase-averaged streamwise velocity, $\langle u(y,z,t)\rangle/U_e$, and r.m.s. velocity fluctuations, $\langle u_t'(y,z,t)\rangle/U_e$, measured at $x/D_e = 2$ at four equal time intervals

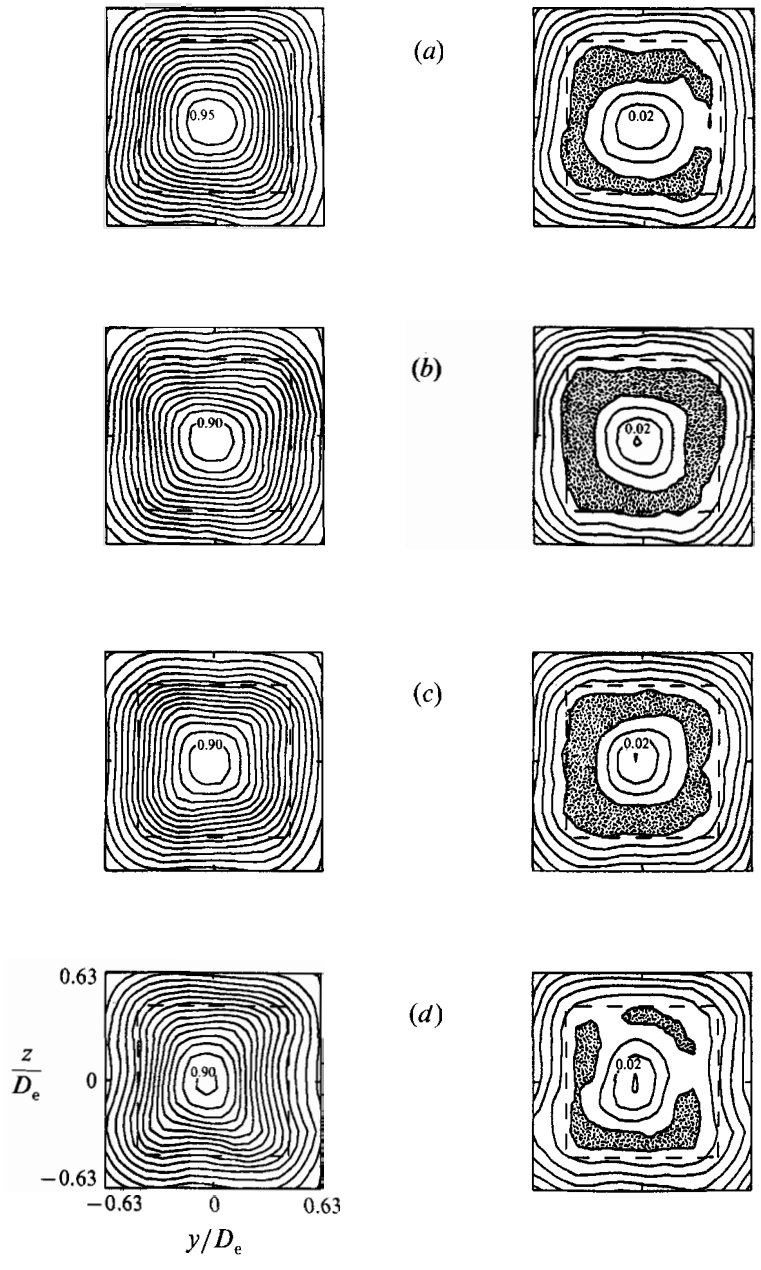

FIGURE 12. Contours of $\langle u(y,z)\rangle/U_e$ (left) and $\langle u_t'(y,z)\rangle/U_e$ (right) measured at $x/D_e = 2$. The jet is forced with P_0 and the contour maps are plotted at four equal time intervals during the modulating period: (*a*) τ_1; (*b*) τ_2; (*c*) τ_3; (*d*) τ_4. Contour increments for $\langle u\rangle/U_e$ and $\langle u_t'\rangle/U_e$ are 0.05 and 0.005, respectively; levels of centre contours are labelled. Regions where $\langle u_t'\rangle/U_e$ is greater than the maximum contour level are shaded.

during the modulation period. These times are referred to below as τ_1, τ_2, τ_3 and τ_4 ($\tau = t/T_f$) and are chosen so that τ_1 corresponds to zero crossings of the reference signal, $e_{ref}(t)$, where $de_{ref}(t)/dt > 0$ and $\tau_i = \tau_1 + (i-1)/4$ ($i = 2$, 3, and 4). When the flow is excited with P_0 (figure 12*a–d*), the jet retains its initial squareness and there are no significant differences between the four contour plots. In similar contour plots

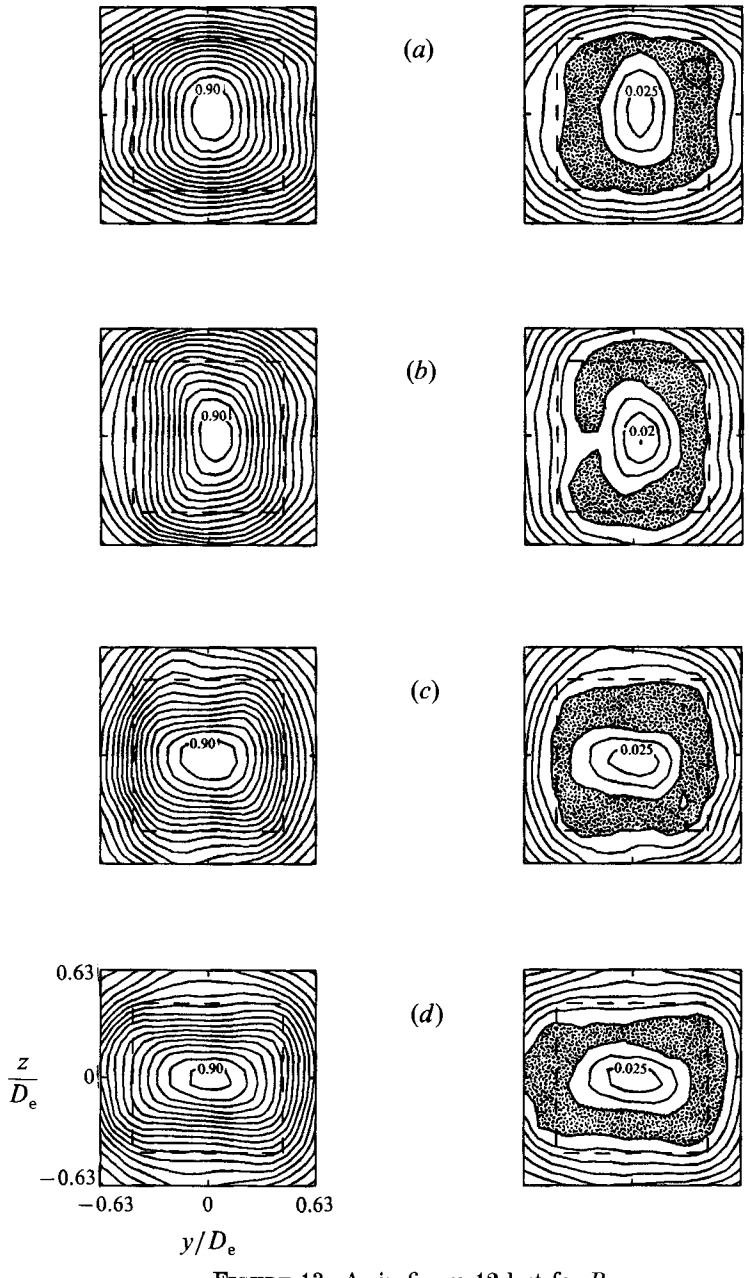

FIGURE 13. As in figure 12 but for $P_{\pm 2}$.

taken at $x/D_e = 4$ (not shown), the jet is considerably more circular, as is evident from figure 10(*c*).

When the flow is forced with $P_{\pm 2}$, the contour maps change substantially during the excitation period. At $\tau = \tau_2$ and τ_4 (figures 13*b* and 13*d*, respectively), the jet cross-section is essentially rectangular, with an aspect ratio in excess of 2. The major axis of this rectangle is clearly aligned with the z- and y-axes at $\tau = \tau_2$ and τ_4, respectively. Thus, the major and minor axes of the cross-section of the forced jet are interchanged during each cycle of the modulating wave train. Recall that for $P_{\pm 2}$ the

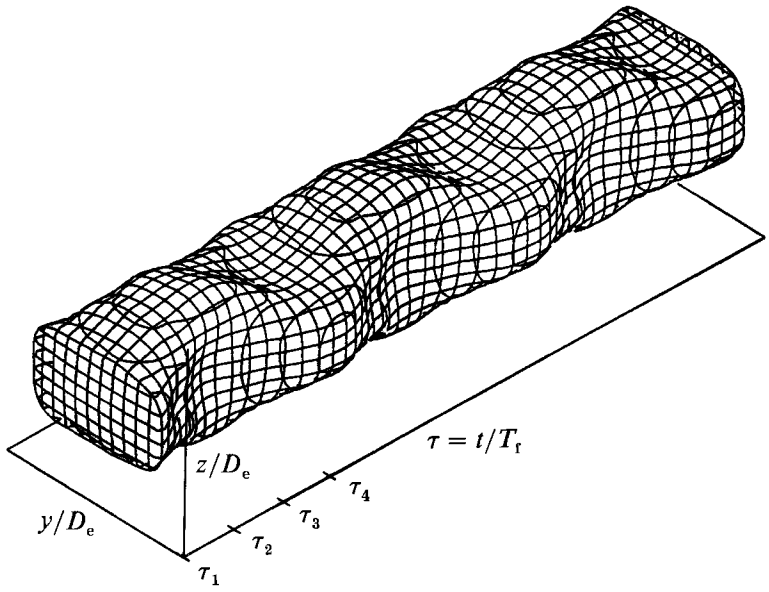

FIGURE 14. The surface $\langle u(y,z,t)\rangle/U_e = 0.625$ at $x/D_e = 2$ during three periods of the modulating waveform of $P_{\pm 2}$ (the τ-coordinate begins at $\tau = \tau_1$, and τ_1, τ_2, τ_3, and τ_4 are marked for reference).

maxima, e_{max}, of the modulating waveforms of each pair of opposite actuators occur at the same time as the minima, e_{min}, of the modulating waveforms of the other pair. The corresponding maxima of the (modulated) excitation input of each pair of opposite actuators are above the threshold at which rollup of the line vortices occurs within the forced azimuthal segments of the jet shear layer. The rollup leads to an increase in the cross-stream spreading of the forced segments and a rectangular distortion of the jet cross-section (cf. figure 11*b*). Note that τ_2 corresponds to $e_m^2 = e_m^4 = e_{max}$, while τ_4 corresponds to $e_m^1 = e_m^3 = e_{max}$.

A noteworthy feature of each of figures 13(*a*) and 13(*c*) is the variation in aspect ratio of contours of $\langle u\rangle/U_e$ and $\langle u_t'\rangle/U_e$. For example, at $\tau = \tau_1$ (figure 13*a*), velocity contours with levels $\langle u\rangle/U_e > 0.5$ are nominally rectangular, with their major axes roughly aligned with the z-axis, while velocity contours with levels $\langle u\rangle/U_e < 0.5$ are nominally rectangular, with their major axes roughly aligned with the y-axis. The contour $\langle u\rangle = 0.5$ is approximately square in figures 13(*a*) and 13(*c*). This indicates that when τ first exceeds τ_2 (or τ_4), the changes in aspect ratio of the velocity contours begin near the centreline of the jet and then propagate toward its outer edges so that when $\tau = \tau_2 + \frac{1}{2}$ (or $\tau_4 + \frac{1}{2}$), the axis switching is completed. The axis switching of the jet for $P_{\pm 2}$ is also shown in an isometric plot of the surface $\langle u\rangle/U_e = 0.625$ in the (y,z,t)-coordinates at $x/D_e = 2$ during three periods of the modulation waveform (figure 14). (The τ coordinate begins at $\tau = \tau_1$, and τ_1, τ_2, τ_3, and τ_4 are marked for reference.)

These changes in aspect ratio are apparently connected with the advection of vortical structures past the measurement station. The three-dimensional features of these structures are captured using phase-averaged concentrations of r.m.s. velocity fluctuations. The utility of this scheme was demonstrated in a transitional plane shear layer by Nygaard & Glezer (1991), who computed $u_t'(\boldsymbol{x},t)$ relative to time series of the instantaneous streamwise velocity. Although concentrations of $\langle u_t'(\boldsymbol{x},t)\rangle$ are not the same as vorticity concentrations, they closely resemble the features of streamwise vortices in the spanwise-forced plane shear layer.

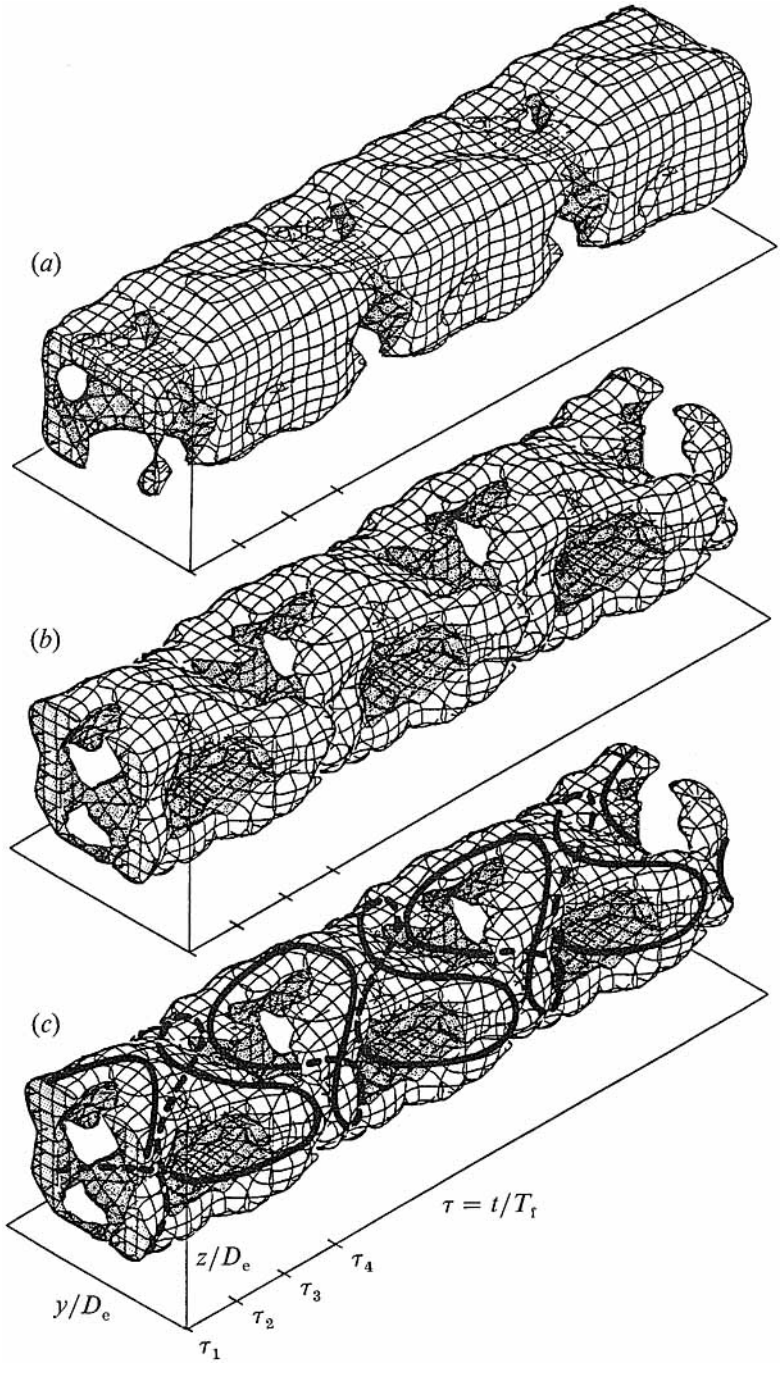

FIGURE 15. The surfaces $\langle u_i'(y,z,t)\rangle/U_e = 0.037$ at $x/D_e = 2$ during three periods of the modulating waveforms of programmes (*a*) P_0 and (*b*) $P_{\pm 2}$. A train of distorted elliptic vortex rings corresponding to (*b*) is illustrated in (*c*).

In figures 15(*a*) and 15(*b*), we show the surfaces $\langle u' \rangle / U_e = 0.037$ in the (y, z, t)-coordinates at $x/D_e = 2$ for P_0 and $P_{\pm 2}$, respectively, during three periods of the modulating waveform (cf. figure 14). When the flow is excited with P_0 (figure 15*a*), the vortical structures appear to be an organized train of square vortex rings that are advected past the measurement station at the modulating frequency. When the flow is excited with $P_{\pm 2}$ (figure 15*b*), the phase-averaged vortical structures are considerably more complex and resemble a train of distorted elliptic vortex rings, as illustrated in figure 15(*c*). We note that the passage frequency of these vortices is *twice* the modulating frequency, and that each pair of adjacent vortices is symmetrically distorted in time about the (y, z)-planes at $\tau_2 + \frac{1}{2}n$ (or $\tau_4 + \frac{1}{2}n$), where n is an integer.

It is well-known that isolated non-circular vortex rings undergo self-induced and roughly time-periodic core deformations as they are advected away from the vortex generators (e.g. Kambe & Takao 1971). In particular, elliptic vortex rings undergo core deformations that lead to time-periodic 'switching' of their major and minor axes (Dhanak & Bernardinis 1981) that has been connected with the streamwise evolution and spatial axes switching of elliptic jets (Ho & Gutmark 1987; Hussain & Husain 1989). The flow visualization photographs of Ho & Gutmark show that near the nozzle of an elliptic jet (aspect ratio 2:1) and upstream of the first axis switching, consecutive elliptic vortices are similarly distorted as they are advected downstream. In photographs taken in planes of the major and minor axes of the elliptic nozzle, these distortions appear as upstream and downstream bends, respectively, about the jet centreline. As argued by Hussain & Husain, these distortions lead to streamwise stretching and compressing of the mean y, z cross-sections of the jet along the minor and major axes of the nozzle, respectively. Axis switching begins when the minor and major axes of the jet are approximately equal in length.

Hussain & Husain (1989) assert that azimuthal variations in momentum thickness of the shear layer of an elliptic jet lead to azimuthally non-uniform rollup of elliptic vortices. The rollup appears to progress azimuthally before the cores of these vortices begin to deform. Hence, we conjecture that when the jet is forced with $P_{\pm 2}$, rollup of two opposite segments of the jet shear layer is alternately initiated by a corresponding pair of opposite actuators (1, 3 and 2, 4) every $\frac{1}{2}T_f$ and then continues azimuthally. Figures 8(*d*) and 8(*f*) suggest that the forced rollup of the two opposite segments of the jet shear layer results in vortices (marked V in these figures) having cross-sections that scale with the width of the jet. The proximity of these vortices apparently forces some of the jet fluid between them to move away from the centreline and parallel to their axes, thus leading to the formation of an almost elliptic vortex ring, the major axis of which is parallel to the tips of the active actuators. Because the two opposite pairs of actuators are activated alternately, the major axes of consecutive elliptical vortices are alternately aligned with either the y- or z-axes. This is consistent with the vortical structures observed at $x/D_e = 2$ as shown in figure 15(*b*, *c*).

Finally, the effect of excitation programmes P_0, $P_{\pm 1}$, $P_{\pm 2}$, and P_{-1} on the jet column (at $x/D_e = 4$) may be inferred from surface plots of $\langle u(y, z, t) \rangle = 2.5$ m/s (figure 16*a–d*). (The plotting routine does not allow for independent scaling of the three coordinates, hence the scaling in the (y, z)-plane of figure 16 is different from the scaling in figures 14 and 15.) As discussed in connection with figure 10(*c*), figure 16(*a*) shows that forcing with P_0 results in a jet cross-section that is virtually circular during most of the excitation period. When the jet is forced with $P_{\pm 1}$ (figure 16*b*), its centre (as may be determined by the maximum streamwise velocity) oscillates

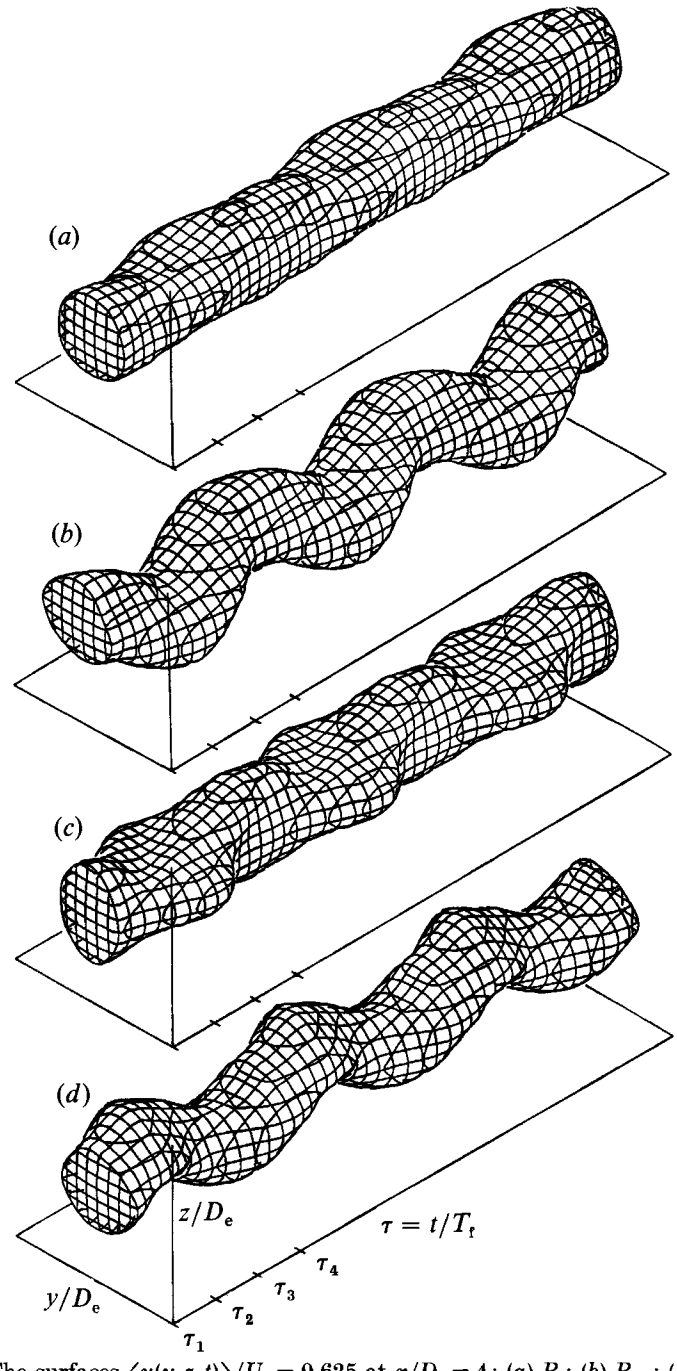

FIGURE 16. The surfaces $\langle u(y,z,t)\rangle/U_e = 0.625$ at $x/D_e = 4$: (*a*) P_0; (*b*) $P_{\pm1}$; (*c*) $P_{\pm2}$; (*d*) P_{-1}.

harmonically (at the excitation frequency) along the line of symmetry of the forcing, which is also a corner bisector of the square conduit. The amplitude of oscillation is $0.16D_e$ relative to the jet centreline. As in figure 14, when the jet is forced with $P_{\pm2}$ (figure 16*c*), its cross-section becomes elliptical, with an aspect ratio that varies time harmonically between 0.5 and 2. When the jet is forced with P_{-1} (figure 16*d*),

its cross-section is almost circular and its centre spins helically with time. The direction of the spin corresponds to instability mode -1 of a round jet.

5. Summary and conclusions

The utility of piezoelectric actuators for the modification of free shear flows has been demonstrated in a square air jet. Velocity perturbations are introduced into the jet shear layer by the motion of the free ends of planar cantilevered actuators driven at their resonance frequency. At low excitation levels, the flow is typically not receptive to excitation at the resonance frequency and its higher harmonics, and the induced velocity perturbations are rapidly attenuated. Although the amplitude of the actuator displacement is less than a millimetre, the magnitude of the induced velocity perturbation is proportional to the product of the actuator displacement and its frequency. Hence, if the resonance frequency is high enough, the induced velocity perturbation can be quite large and lead to the rollup of line vortices with axes parallel to the actuator tip within forced azimuthal segments of the jet shear layer. These vortices are formed at the resonance frequency of the actuator, and their cross-sectional dimension scales with the actuator's displacement.

Farther downstream from the actuators, the line vortices coalesce and rapidly lose their identity, rendering velocity spectra of the forced flow virtually featureless. Nevertheless, the formation of these vortices is accompanied by a substantial increase in the cross-stream spreading of the forced segments of the jet shear layer. Hence, excitation at the resonance frequency with azimuthally non-uniform amplitude distribution can result in a substantially distorted mean flow having a featureless velocity spectrum. This capability suggests that proper selection of input waveforms can be used to tailor the mean velocity profile as to provide favourable conditions for the introduction and propagation of desirable low-frequency disturbances.

Because the line vortices appear only when the induced velocity perturbations exceed a given threshold, amplitude modulation of the excitation waveform results in their rapid coalescence into larger vortical lumps at the modulating frequency. This means that by resonantly driving the actuators with a time-harmonic carrier wave train that is amplitude modulated with the desired excitation input, the excitation waveform can be effectively demodulated by the flow. As a result, the flow is primarily affected by the modulating wave train, while velocity perturbations at the resonance frequency and its higher harmonics are attenuated. Thus, the excitation waveform is tailored to the flow, providing a much more flexible approach than matching the resonance frequency of the actuators to the receptivity of the flow.

The substantial increase in the spreading of forced azimuthal segments of the jet shear layer in the absence of low-frequency modulation suggests itself as a mechanism by which various azimuthal instability modes of the jet column can be effectively excited. This attribute may be particularly useful when the shear layer of the unforced jet is extremely thin, as is the case for high-speed jets where, for a given Strouhal number, there can be a substantial mismatch between unstable frequencies of the jet column and of the jet shear layer.

In the present experiments, the jet is forced by amplitude modulation of the signals resonantly driving each of four piezoelectric actuators placed around the jet exit. The modulating waveforms are time harmonic, have the same frequency, and their relative phases are programmable. The four azimuthal excitation programmes

of the present experiments, P_0, $P_{\pm1}$, $P_{\pm2}$, and P_{-1}, correspond to lowest order to excitation of azimuthal modes $m = 0$, ±1, ±2, and -1, respectively, of an axisymmetric jet. (The presence of strong modal components at these azimuthal wavenumbers was verified by modal decomposition of streamwise velocity data for each excitation programme.) These excitation programmes also result in substantial distortions of cross-sections of the jet in the (y, z)-plane. Of particular note are $P_{\pm1}$, which results in an oval cross-section having a major axis along the jet's corner bisector, and $P_{\pm2}$, which leads to a cross-section having an approximate fourfold symmetry with respect to the y- and z-axes.

Contours of phase-averaged streamwise velocity in the (y, z)-plane have shown that when the jet is forced with $P_{\pm2}$, the major and minor axes of its cross-section at a given streamwise station are continuously interchanged every half period of the modulating wave train. The reduction (or increase) in a given maximum (or minimum) cross-sectional aspect ratio begins near the centreline of the jet and propagates toward its outer edges to complete the axis switching. These changes in aspect ratio are apparently connected with the advection of distorted elliptic vortical structures past the measurement station.

The authors are grateful to Professor F. H. Champagne for making parts of the jet facility and the traversing mechanism available for the present experiments. The Schlieren system described in the manuscript was constructed by Mr S. M. Green, who also assisted in obtaining the Schlieren photographs. This work has been supported by AFOSR Grant 89-0465, monitored by Dr J. M. McMichael.

REFERENCES

Berger, E. 1967 Suppression of vortex shedding and turbulence behind oscillating cylinders. *Phys. Fluids Suppl.* S191–S193.

Betzig, R. E. 1981 Experiments on the linear and non-linear evolution of the double helical instability in jets. *AIAA Paper* 81-0415.

Champagne, F. H., Pao, Y. H. & Wygnanski, I. J. 1976 On the two-dimensional mixing region. *J. Fluid Mech.* **74**, 209–250.

Crow, S. C. & Champagne, F. H. 1971 Orderly structure in jet turbulence. *J. Fluid Mech.* **48**, 547–591.

Dhanak, M. R. & Bernardinis, B. 1981 The evolution of an elliptic vortex ring. *J. Fluid Mech.* **109**, 189–216.

DuPlessis, M. P., Wang, R. L. & Kahawita, R. 1974 Investigation of the near-region of a square jet. *Trans. ASME* I: *J. Fluids Engng* **96**, 246–251.

Gessner, F. B., Po, J. K. & Emery, A. F. 1977 Measurements of developing turbulent flow in a square duct. In *Proc. Symp. on Turbulent Shear Flows, Pennsylvania State Univ., April 18–20, 1977*, pp. 119–136. Pennsylvania State University.

Glezer, A., Katz, Y. & Wygnanski, I. 1989 On the breakdown of the wave packet trailing a turbulent spot in a laminar boundary layer. *J. Fluid Mech.* **198**, 1–26.

Gutmark, E., Schadow, K. C., Parr, T. P., Hanson-Parr, D. M. & Wilson, K. J. 1989 Non-circular jets in combustion systems. *Exps Fluids* **7**, 248–258.

Gutmark, E., Schadow, K. C., Parr, D. M., Harris, C. K. & Wilson, K. J. 1985 The mean and turbulent structure of noncircular jets. *AIAA Paper* 85-0543.

Ho, C.-M. & Gutmark, E. 1987 Vortex induction and mass entrainment in a small-aspect-ratio elliptic jet. *J. Fluid Mech.* **179**, 383–405.

Ho, C.-M. & Huang, L.-S. 1982 Subharmonic and vortex merging in mixing layers. *J. Fluid Mech.* **119**, 443–473.

Ho, C.-M. & Huerre, P. 1984 Perturbed free shear layers. *Ann. Rev. Fluid Mech.* **16**, 365–424.

HUSSAIN, F. & HUSAIN, H. S. 1989 Characteristics of unexcited and excited jets. *J. Fluid Mech.* **208**, 257–320.

KAMBE, T. & TAKAO, T. 1971 Motion of distorted vortex rings. *J. Phys. Soc. Japan* **31**, 591–599.

LEE, M. & REYNOLDS, W. C. 1985 Bifurcating and blooming jets. *Rep.* TF-22. Stanford University.

LIEPMANN, H. W., BROWN, G. L. & NOSENCHUCK, D. M. 1982 Control of laminar instability waves using a new technique. *J. Fluid Mech.* **118**, 187–200.

LIEPMANN, H. W. & NOSENCHUCK, D. M. 1982 Active control of laminar-turbulent transition. *J. Fluid Mech.* **118**, 201–204.

LONG, T. A. & PETERSEN, R. A. 1992 Controlled interactions in a forced axisymmetric jet. Part 1. The distortion of the mean flow. *J. Fluid Mech.* **235**, 37–55.

MELLING, A. & WHITELAW, J. H. 1976 Turbulent flow in a rectangular duct. *J. Fluid Mech.* **78**, 289–315.

NYGAARD, K. J. & GLEZER, A. 1991 Evolution of streamwise vortices and generation of small-scale motion in a plane shear layer. *J. Fluid Mech.* **231**, 257–301.

OSTER, D. & WYGNANSKI, I. 1982 The forced mixing layer between parallel streams. *J. Fluid Mech.* **123**, 91–130.

OSTER, D., WYGNANSKI, I. & FIEDLER, H. 1977 Some preliminary observations on the effect of initial conditions on the structure of the two-dimensional turbulent mixing layer. In *Turbulence in Internal Flows* (ed. S. N. B. Murthy), pp. 67–87. Hemisphere.

QUINN, W. R. & MILITZER, J. 1988 Experimental and numerical study of a turbulent free square jet. *Phys. Fluids* **31**, 1017–1025.

REISENTHEL, P. 1988 Hybrid instability in an axisymmetric jet with enhanced feedback. Ph.D. dissertation, Illinois Institute of Technology, Chicago.

ROBERTS, F. A. & ROSHKO, A. 1985 Effects of periodic forcing on mixing in turbulent shear layers and wakes. *AIAA Shear Flow Control Conf., March 12–14, Boulder, Colorado.*

SCHUBAUER, G. B. & SKRAMSTAD, H. K. 1947 Laminar boundary layer oscillations and stability of laminar flow. *J. Aero. Sci.* **14**, 68–78.

SFORZA, P. M., STEIGER, M. H. & TRENTACOSTE, N. 1966 Studies on three-dimensional viscous jets. *AIAA J.* **4**, 800–806.

STRANGE, P. J. R. & CRIGHTON, D. G. 1983 Spinning modes in axisymmetric jets. Part 1. *J. Fluid Mech.* **134**, 231–245.

TRENTACOSTE, N. & SFORZA, P. M. 1967 Further experimental results for three-dimensional free jets. *AIAA J.* **5**, 885–891.

TSUCHIYA, Y., HORIKOSHI, C. & SATO, T. 1986 On the spread of rectangular jets. *Exps Fluids* **4**, 197–204.

WEHRMANN, O. H. 1965 Reduction of velocity fluctuations in a Kármán vortex street by a vibrating cylinder. *Phys. Fluids* **8**, 760–761.

WEHRMANN, O. H. 1967*a* The influence of vibrations on the flow field behind a cylinder. *Document* D1-82-0619. Boeing Scientific Research Laboratories.

WEHRMANN, O. H. 1967*b* Self-adjusting feedback loop for mechanical systems to influence flow in transition. Part I. *Document* D1-82-0632. Boeing Scientific Research Laboratories.